Kidney-specific claudin-2 deficiency leads to medullary nephrocalcinosis in mice

Christine Behm¹, Duuamene Nyimanu¹, Ony Araujo Galdino^{2, 5}, Sadhana Kanoo², Young Chul Kim², Natalia Lopez², Helen Goodluck², Peter S. Rowe¹, Andrew P. Evan³, André J. Sommer³, Matthew N. Barr⁴, Tracy Punshon⁴, Volker Vallon², Brian P. Jackson⁴, James C. Williams³, Alan S. L. Yu¹

¹Division of Nephrology and Hypertension, Department of Internal Medicine, and the Jared Grantham Kidney Institute, University of Kansas Medical Center, Kansas City, KS

²Division of Nephrology and Hypertension, Department of Medicine, University of California San Diego, La Jolla, CA, and VA San Diego Healthcare System, San Diego, CA

³Department of Anatomy, Cell Biology & Physiology, Indiana University School of Medicine, Indianapolis, IN

⁴Biomedical National Elemental Imaging Resource, Department of Earth Sciences, Dartmouth College, Hanover, NH

⁵Current address: Department of Clinical and Toxicological Analyses, Federal University of Rio Grande do Norte (UFRN), Natal, RN, Brazil

Keywords: Hypercalciuria, tight junction, renal tubule, kidney stone, ICP-MS

Running head: Nephrocalcinosis in Cldn2 knockout mice

Abstract: 182 words Word count: 8985

Contact author:

Alan S. L. Yu, MB, BChir Division of Nephrology and Hypertension University of Kansas Medical Center 3901 Rainbow Blvd, 6018 WHE Kansas City, KS 66160-3018

Tel: (913) 588 9252 Fax: (913) 588 9251

Conflict of interest statement:

ASLY has served as a consultant or advisory board member for Regulus, Calico, Sarepta, Travere, Torque Bio and Estuary and received royalties from Elsevier and Wolters-Kluwer.

ABSTRACT

Deposits of hydroxyapatite called Randall's plaques are found in the renal papilla of calcium oxalate kidney stone formers and likely serve as the nidus for stone formation, but their pathogenesis is unknown. Claudin-2 is a paracellular ion channel that mediates calcium reabsorption in the renal proximal tubule. To investigate the role of renal claudin-2, we generated kidney tubule-specific claudin-2 conditional knockout mice (KS-Cldn2 KO). KS-Cldn2 KO mice exhibited transient hypercalciuria in early life. Normalization of urine calcium was accompanied by a compensatory increase in expression and function of renal tubule calcium transporters, including in the thick ascending limb. Despite normocalciuria, KS-Cldn2 KO mice developed papillary hydroxyapatite deposits, beginning at 6 months of age, that resembled Randall's plaques and tubule plugs. Bulk chemical tissue analysis and laser ablation-inductively coupled plasma mass spectrometry revealed a gradient of intrarenal calcium concentration along the corticomedullary axis in normal mice, that was accentuated in KS-Cldn2 KO mice. Our findings provide evidence for the "vas washdown" hypothesis for Randall's plaque formation, and identify the corticomedullary calcium gradient as a target for therapies to prevent kidney stone disease.

SUMMARY

Knockout of the claudin-2 gene in kidneys of mice leads to increase in medullary calcium concentration gradient and deposition of mineral in the renal papilla.

INTRODUCTION

The incidence of kidney stone disease has been increasing steadily and lifetime risk is now estimated to exceed 22% in males and 15% in females (1). The most common type of kidney stone is calcium oxalate, and idiopathic hypercalciuria (IH) is its major risk factor (2). IH is heritable and polygenic, and due to the combined effect of intestinal hyperabsorption of calcium (3), renal calcium wasting (4, 5), and bone calcium resorption (6). An important initial pathogenic step is the deposition in the medullary interstitium of calcium phosphate mineral in the form of hydroxyapatite, known as Randall's plaques (7-9). These grow over time and rupture through the papillary epithelium into the urinary space, exposing a nidus for the precipitation and growth of calcium oxalate stones.

In the kidney, the majority of filtered calcium (70%) is reabsorbed in the proximal tubule (PT). Transcellular reabsorption of sodium and water in the PT leads to a rise in the luminal calcium concentration that, together with the lumen-positive transepithelial voltage in the late PT, provides the driving force for passive diffusion of calcium via the paracellular pathway (10, 11). Claudins are tight junction membrane proteins that function as paracellular channels. Claudins 2 and 12 are the predominant calcium-permeable paracellular channels in the PT. Global, constitutive knockout of the claudin-2 gene (*Cldn2*) in mice (12), or double-knockout of both *Cldn2* and *Cldn12* (13), lead to hypercalciuria.

Curry *et al.* showed that the hypercalciuria in constitutive *Cldn2* knockout mice was caused by both renal calcium leak and primary intestinal hyperabsorption of calcium (12). Constitutive *Cldn2* knockout mice also exhibited papillary deposits of hydroxyapatite. Thus, constitutive *Cldn2* knockout mice phenocopy the early pathogenic steps in human IH and kidney stone disease. Furthermore, common, non-coding variants in the human *CLDN2* gene were found to be associated with an increased risk of kidney stone disease in the general population, and a rare missense mutation in *CLDN2* was discovered in one family with an X-linked syndrome of hypercalciuria, kidney stone disease and male infertility (12).

Claudin-2 is highly expressed not only in the kidney, but also throughout the intestinal epithelium. To elucidate the role of kidney claudin-2 in the pathogenesis of hypercalciuria and kidney stone disease, we generated floxed *Cldn2* mice, and developed renal tubule-specific *Cldn2* conditional knockout mouse models.

RESULTS

Generation and characterization of kidney-specific claudin-2 knockout mice

We crossed *Cldn2* floxed mice with Pax8-Cre to generate constitutive kidney-specific *Cldn2* knockout mice. *Cldn2* was efficiently deleted from both the PT and the thin descending limbs (Fig. 1A–C). Claudin-2 has been shown to mediate PT paracellular Na⁺ reabsorption. Consistent with this, the glomerular filtration rate (GFR) was reduced in the knockout mice compared to control littermates (Fig. 1D), presumably due to increased Na⁺ delivery to the macula densa, activating tubuloglomerular feedback. We used clearance of lithium, a monovalent alkali cation like Na⁺ that is reabsorbed predominantly in the PT, to assess PT reabsorptive function. Urinary excretion of lithium was no different between knockout mice and controls, but because GFR was reduced, the fractional excretion of lithium was increased (Fig. 1E). This demonstrates that PT reabsorption of Na⁺, and potentially other cations, is impaired with *Cldn2* knockout. Systolic blood pressure was also reduced in the *Cldn2* knockout mice (Fig. 1F), presumably due to loss of total body Na⁺.

Kidney-specific claudin-2 knockout causes transient hypercalciuria

To test the hypothesis that claudin-2 in the renal tubule regulates urine calcium excretion, we measured urine calcium excretion in constitutive kidney-specific *Cldn2* knockout mice. Constitutive knockout mice were hypercalciuric at weaning, but their urine calcium decreased with age and was similar to controls by 6–8 weeks (Fig. 2A). By contrast, global, constitutive *Cldn2* knockout mice, which we previously reported to be hypercalciuric (12), showed increased urine calcium throughout adulthood up to 2 years of age (Fig. 2B). This suggests that kidney-specific *Cldn2* knockout mice are able to fully compensate for the defect in paracellular calcium reabsorption with age, whereas global *Cldn2* knockout mice are not.

To confirm that deletion of *Cldn2* causes hypercalciuria due to a functional transport defect and not due to a developmental abnormality, we generated inducible kidney-specific *Cldn2* knockout mice by crossing claudin-2 floxed mice to Pax8-LC1 ("Tet-On") mice (Suppl. Fig. S1). After induction with oral doxycycline for one week, claudin-2 protein was no longer detectable in whole kidney lysates by immunoblotting and in PT by immunofluorescence, whereas claudin-2 was well expressed in control mice with omission of the Pax8 or LC1

transgene, or treated with vehicle (Fig. 3A, B). Claudin-2 is normally also expressed in the upper segments of the thin descending limbs of long-looped nephrons. However, in these mice doxycycline induced only a partial deletion of *Cldn2* from thin descending limbs (Fig. 3B, lower panels), which was due to inefficient Cre recombination (Suppl. Fig. S2). Nevertheless, treatment of 5 week-old inducible knockout mice with 1 week of doxycycline induced a 2.5-fold increase in urine calcium/creatinine ratio, demonstrating that PT claudin-2 is essential for tubular calcium reabsorption (Fig. 3C).

Compensatory upregulation of parathyroid hormone (PTH) and thick ascending limb and distal convoluted tubule calcium transport mechanisms in response to loss of kidney claudin-2

We previously showed in global claudin-2 knockout mice that renal calcium loss was matched by primary intestinal hyperabsorption of calcium, leading to even total body calcium balance. We therefore predicted that knockout of Cldn2 in the renal tubule but not the intestine would lead to negative calcium balance and be reflected in compensatory hormonal changes. We found that serum calcium was unchanged (Fig. 4A), but PTH was increased in kidney-specific Cldn2 knockout mice by 1.5-fold (males) to 2-fold (females) compared to controls (Fig. 4B, P = 0.0008), as would be expected in response to calcium wasting. There was no change in 1,25-dihydroxyvitamin D levels (Fig. 4C). Bone mineral density at the lumbar spine and femur, or summed over the whole body (Fig. 4D) tended on average to be lower in the knockout mice at all ages, but this did not reach statistical significance.

To determine if defective PT calcium reabsorption was compensated by upregulation of other calcium transporters, we quantitated their mRNA levels by qPCR at 4 weeks (when the kidney-specific *Cldn2* knockout mice were hypercalciuric), 10 weeks (when they were no longer hypercalciuric) and 1 year of age (Fig. 5). The major PTH-regulated calcium transport proteins in the distal convoluted tubule, TrpV5, calbindin D28k and NCX1 (14), were all significantly upregulated in kidney-specific *Cldn2* knockout mice. Likewise, the major calcium transport proteins in the thick ascending limb of Henle (NKCC2, claudin-16 and claudin-19) were significantly upregulated. Although claudin-12 has been shown to contribute to renal calcium reabsorption in the proximal tubule, we observed no compensatory upregulation of claudin-12. There was also no change in the expression of claudin-14, the plasma membrane calcium ATPase, PMCA1, and the hydroxylase enzymes for activation and inactivation of vitamin D (Cyp27b1, Cyp24a1).

To test functionally for compensatory upregulation of reabsorption in the thick ascending limb of Henle and the distal convoluted tubule, diuretic challenge assays were performed in 12 week-old mice using a loop diuretic, furosemide, and a thiazide diuretic, hydrochlorothiazide (Fig. 6A). Over the 4 hour period after furosemide administration, urine volume and urine sodium excretion were increased equally in kidney-specific Cldn2 knockout and control mice (Fig. 6B). Urine calcium excretion was also increased with furosemide, with female mice exhibiting greater calciuresis. Importantly, calcium excretion was increased to a greater extent in kidney-specific Cldn2 knockout mice compared to controls with a least-squares mean difference (\pm SE) of 0.39 \pm 0.19 g/g (P = 0.039 for genotype*treatment interaction).

The increase in sodium excretion with hydrochlorothiazide treatment compared to vehicle was greater in the knockout mice than controls, with a least-squares mean difference (\pm SE) of 1.32 \pm 0.59 μ mol/g body weight/hr (P = 0.03 for genotype*treatment interaction). Hydrochlorothiazide is not expected to block Ca reabsorption in distal convoluted tubule and actually decreased urine calcium excretion with no significant difference between knockout and control mice (Fig. 6C).

Nephrocalcinosis in older mice despite normocalciuria

We previously reported that global *Cldn2* knockout mice, which are hypercalciuric throughout life, exhibit papillary nephrocalcinosis. Surprisingly, despite the fact that kidney-specific *Cldn2* knockout mice were normocalciuric throughout their adult life, they also develop medullary nephrocalcinosis. By histological staining and micro-computed tomography scanning, we observed linear inner medullary deposits of calcium mineral, densely concentrated in the papilla, that began from 6–8 months of age in females and 12 months in males (Fig. 7). A majority of deposits were intraluminal while a few large, flat-shaped deposits were seen in the interstitium (Fig. 7C). By infrared spectroscopy, the composition of the deposits was determined to be predominantly calcium phosphate in the form of apatite, with some calcium carbonate (Fig. 7D). Importantly, this occurred despite KS-*Cldn2* KO mice being normocalciuric from 6 weeks of age. Thus, there is a striking dissociation in these mice between urine calcium excretion and kidney tissue mineral deposition.

Discovery of a corticomedullary calcium gradient

The finding that kidney-specific *Cldn2* knockout mice develop papillary nephrocalcinosis despite normocalciuria suggests that their normal urine calcium might be masking an accumulation of calcium within the medullary tissue. Our finding that these mice have compensatory thick ascending limb reabsorption of calcium provides the mechanistic basis for this. Mathematical modeling has predicted the existence of a corticomedullary interstitial gradient of calcium in the normal kidney (15). Moreover, in IH stone-formers, who also have a defect in PT calcium reabsorption (16-18), it has been hypothesized that the increased delivery of calcium from the PT to the loop of Henle, and the increased reabsorption of calcium from the thick ascending limb, leads to greater concentration of calcium in the inner medullary interstitium and papilla due to the vasa recta blood flow and countercurrent exchange, which has been called the "vas washdown" hypothesis (19).

To test this hypothesis, we determined the axial distribution of calcium content in the kidney in mice at a sufficiently early age that mineral deposits were not yet detectable (16–17 weeks). The kidneys were dissected into cortex, medulla and papilla, bulk tissue calcium extracted by two different methods, and calcium content quantitated (Fig. 8A). Calcium concentration using the acid ash method, which measures total mineral content, was approximately 5-fold higher than by the diffusible calcium method. However, both methods revealed a similar relative calcium distribution with higher calcium concentration in the papilla than in the cortex and medulla (Fig. 8B). Given the decreased PT calcium reabsorption in kidney-specific Cldn2 knockout mice and compensatory upregulation of the function and expression of the thick ascending limb calcium transporters, we predicted that the corticomedullary calcium gradient would be exacerbated. Indeed, we found that papillary calcium concentration was greater in kidney-specific Cldn2 knockout mice than in controls. This was more marked in female mice (least-squares mean difference (\pm SE) of 0.043 mg/g wet weight, P < 0.0001) and significantly attenuated in males (least-squares mean difference (\pm SE) of 0.014 \pm 0.056 mg/g wet weight, P = 0.8). Moreover, the results were similar whether calcium content was expressed relative to wet weight or to dry weight of tissue (Fig. 8C, D). In older animals (26 weeks), the accumulation of papillary calcium in kidney-specific Cldn2 knockout mice was even more striking and occurred independent of sex (Suppl. Fig. S3).

Spatial distribution of intrarenal calcium

To visualize the 2D spatial distribution of calcium within the kidney at higher resolution, elemental analysis was performed on flash-frozen mouse kidney sections by laser ablation inductively coupled plasma time-of-flight mass spectrometry (LA-ICP-TOFMS). This is a highly sensitive analytical technique in which a laser scans small areas of the tissue section, creating an aerosol that is then introduced into high temperature plasma. The plasma vaporizes and ionizes the particles, and the mass spectrometer separates and detects these ions based on their mass-to-charge ratio.

Studies were performed in mice at 6 weeks old, before the development of mineral deposits. The distribution of sodium, which is known to exhibit a corticomedullary gradient, was used as a positive control. A corticomedullary gradient for calcium was observed, and the gradient for sodium was confirmed (Fig. 9A, Suppl. Fig. 4, 5). By contrast, phosphorus concentration was uniformly distributed throughout the kidney (Suppl. Fig. 6, 7) and other elements showed distinctly different distributions (Suppl. Fig. 7). The ratio of the calcium concentration at the papillary tip to that in the superficial cortex was 3.36 ± 0.50 (mean \pm SD) in control (Cre–) mice, and 15.20 ± 32.23 (mean \pm SD) in kidney-specific *Cldn2* knockout (Cre+) mice (Supplemental Table 1). Calcium appeared to increase exponentially with distance from cortex to medulla (Fig. 10). When log-transformed calcium concentration was fitted to a linear mixed model, the calcium concentration slope as a function of distance was approximately two-fold greater in Cre+ compared to Cre– mice (P = 0.02 for the distance x genotype interaction, Supplemental Table 2). With high resolution mapping (Fig. 9B), the calcium distribution in the papilla did not localize to tubule- or vascular-like structures, but appeared homogeneous. Overlay with immunofluorescently stained adjacent sections for the collecting duct (aquaporin 2, AQP2) and descending thin limbs (aquaporin 1, AQP1) did not show any suggestion of selective colocalization.

DISCUSSION

In summary, we have created a mouse model with conditional kidney-specific knockout of claudin-2 that exhibits medullary deposition of hydroxyapatite despite normocalciuria. Our findings suggest that impaired proximal tubule paracellular calcium reabsorption in these mice is compensated by increased PTH secretion and by upregulation of transcellular and paracellular calcium transporters in the thick ascending limb, as well as the distal convoluted tubule. Our data are consistent with the hypothesis that increased tubule delivery of

calcium to the loop of Henle and compensatory increase in reabsorption of calcium into the medullary interstitium is maladaptive, and leads to the development of medullary nephrocalcinosis.

This mouse model illustrates a dissociation between urine calcium excretion and kidney tissue mineral deposition. Hypercalciuria and increased urinary supersaturation of calcium salts is conventionally thought to be the major causal risk factor for nephrocalcinosis. However, in contrast to claudin-2 knockout mice, mice with genetically defective calcium reabsorption in the thick ascending limb and distal convoluted tubule have little or no nephrocalcinosis despite much more severe hypercalciuria (20-24) (Suppl. Table 3). Likewise, rats bred for 56 generations to excrete 8- to 10-times as much urine calcium as controls nevertheless exhibit no kidney mineral deposits whatsoever (25). Conversely, thick ascending limb-specific knockout of claudin-10 reduces fractional excretion of calcium, presumably by increasing thick limb reabsorption of calcium, and leads to outer medullary nephrocalcinosis despite hypocalciuria (26). These observations are all consistent with a model in which reabsorption of calcium in the loop of Henle is the key determinant of nephrocalcinosis. We suggest that the proximal tubule site for the defect in calcium transport in claudin-2 mice is unique in increasing delivery of calcium to the loop of Henle, where it both accumulates in the lumen and is reabsorbed and deposited in the interstitium.

A key prediction of our pathogenic model was that the kidneys would have a corticomedullary interstitial gradient for calcium, analogous to the gradient for sodium chloride and urea. The existence of such a gradient in the normal kidney was previously predicted by mathematical modelling (15). Moreover, reports of regional calcium content measurements in the older literature in dogs (27) and in human kidneys (28, 29) suggested that the normal renal papilla is enriched in calcium. In our study, we were able to confirm this and visualize a corticomedullary gradient for calcium, using two complementary approaches. Bulk tissue chemical analysis showed higher calcium concentration in the papilla, while spatial fine mapping by mass spectrometry showed a continuous axial corticomedullary calcium gradient. Our method of bulk chemical analysis was clearly very crude compared to LA-ICP-TOFMS, which may well explain the different results. The preparation time (and hence time for diffusion) was longer (2 minutes of dissection vs. snap freezing tissue in seconds), the spatial resolution was poorer (millimeter vs. 2–6 µm resolution) and the sensitivity was less (50 ppm vs. sub-ppm). Additionally, we hypothesized that claudin-2 knockout mice would have increased papillary calcium sequestration, which was indeed the case.

Our findings are important because we believe claudin-2 knockout mice model the development of Randall's plaques, which is a key step in the pathogenesis of human calcium oxalate urinary stones (30, 31). The mineral deposits in claudin-2 knockout mice, like Randall's plaques, are concentrated in the papilla and composed predominantly of hydroxyapatite (8, 32). Like claudin-2 knockout mice, kidney stone formers with idiopathic hypercalciuria have a defect in proximal tubule calcium reabsorption (16, 18). The "vas washdown" model hypothesizes that increased calcium delivery to the loop leads to increased reabsorption of calcium into the medullary interstitium, where the descending vasa recta serve to convey that calcium towards the inner medulla, raising the supersaturation of calcium phosphate to a sufficiently high level in the papilla to deposit as hydroxyapatite (33). The credibility of this model is bolstered by the observation that multiple common variants and one rare missense mutation in the human claudin-2 gene are associated with kidney stone disease (12). The implication of this is that the pathways that lead to papillary calcium deposition may be therapeutic targets for kidney stone disease.

One caveat to this is that our mice differ from the canonical description of Randall's plaques in idiopathic hypercalciuric stone formers in that they have not only medullary interstitial hydroxyapatite deposits, but also tubule plugs. Moreover, when we examine mice by LA-ICP-MS before the development of hydroxyapatite deposits, the distribution of papillary calcium appears homogeneous, suggesting that the increased calcium concentration in the papilla is equilibrated between the interstitium and the tubules. This is not altogether surprising since our model predicts that there should be more calcium delivered to *both* the tubule lumen of the loop of Henle and the surrounding medullary interstitium. Moreover, even in calcium oxalate stone formers, interstitial plaques have been reported to frequently co-occur together with intratubular plugs of mineral (34, 35).

A number of interesting observations in our study deserve brief comment. We found that doxycycline induction of the Pax8-LC1 Cre (sometimes referred to as Pax8rtTA;TetO-Cre) was incomplete and excluded the thin descending limb. Despite this, inducible claudin-2 knockout had robust hypercalciuria. This is consistent with the accepted view that the thin descending limb is impermeable to calcium and presumably plays minimal role in calcium reabsorption (36). However, it raises the intriguing question of what the functional role of claudin-2 is in this nephron segment, given that it is the site with the highest level of claudin-2 expression (37).

Our finding that the kidney-specific claudin-2 knockout mice are able to compensate for defective proximal tubule calcium reabsorption and normalize urine calcium by 6 – 8 weeks of age, whereas the global knockout mice could not, supports the idea that the global knockout mice have intestinal hyperabsorption of calcium and are in positive calcium balance, so that PTH and other compensatory mechanisms are in part suppressed. That the kidney-specific knockouts are transiently hypercalciuric early in life may be due to the sequelae of the large calcium load from suckling, developmental changes in calcium transporter expression, or just the time taken for compensatory increases in gene expression to occur. We did not directly test the mechanism for upregulation of expression of calcium transport proteins in kidney-specific claudin-2 knockout mice but several are known to be upregulated by PTH, including TrpV5, calbindin D28k and NCX1 (14).

We did not identify any significant sex differences in hypercalciuria in our mice. Claudin-2 expression is higher in males than females (38, 39), and we also observed this in our mice once they reached adulthood (Fig. 1b). Thus, one might expect more severe consequences of gene knockout in male mice, including worse hypercalciuria and, if there is more delivery of calcium to the loop, more nephrocalcinosis, but this was not the case. In fact, papillary mineral deposition occurred earlier in female knockout mice. One explanation for this is that the burden of sodium reabsorption is redistributed from the proximal to the distal nephron in females (39). We observed a non-significant trend towards greater natriuresis in response to furosemide in females compared to males, and a significantly greater calciuresis (Fig. 6b). This suggests that increased reabsorption of calcium in the outer medulla may lead to earlier accumulation of interstitial deposits in the female mice. The clinical significance of this is uncertain, however, as we found no sex difference in the association of *CLDN2* common variants with kidney stones in our previous genome-wide association study (12).

We had predicted that the kidney-specific knockout mice would be in negative calcium balance, which would be evident from higher PTH and 1,25-vitamin D levels and lower bone mineral density. We did indeed observe a clear increase in PTH, but 1,25-vitamin D levels were not elevated. This has also been observed in the claudin-2 and claudin-12 double knockout mice, despite more severe hypercalciuria, and raises the intriguing question of whether claudin-2 in the proximal tubule is needed in some way for 1-hydroxylation of 25-hydroxyvitamin D (13). The lack of significant depletion of bone density is not too surprising. The kidney-specific claudin-2 knockout mice are hypercalciuric very transiently in early life and so their cumulative total body calcium deficit is likely to be quite minimal.

The main strengths of our study are that we are able to isolate the role of claudin-2 in the renal tubule by using tissue-specific gene knockout, and we can corroborate our findings with two different Cre lines. One weakness is that we were unable to do calcium balance studies because the mice were very young and hence too small to study during the transient period of hypercalciuria.

In conclusion, kidney-specific claudin-2 knockout mice are normocalciuric other than a transient period of hypercalciuria in early life, yet develop papillary nephrocalcinosis with advanced age. We propose that this represents a model of Randall's plaques, and that it supports the vas washdown theory. Developing therapies to target this mechanism may be an innovative approach to the prevention of kidney stones, and our mice may be a useful model in which to test these.

METHODS

Sex as a biological variable

Our study examined male and female animals, and sex-dimorphic effects are reported.

Generation of kidney-specific claudin-2 knockout mouse

To generate claudin-2 conditional knockout mice, we targeted the *Cldn2* gene on the X chromosome by homologous recombination to insert LoxP sites flanking the single coding exon (inGenious, Ronkonkoma, NY), as depicted in Supplemental Fig. S1. The mice were then backcrossed for 10 generations onto the C57BL6/J background. Constitutive kidney-specific *Cldn2* knockout mice were generated by crossing *Cldn2* floxed mice (*Cldn2*^{fl/fl} or *Cldn2*^{fl/gl}) with Pax8-Cre knock-in mice, which express Cre constitutively throughout the renal tubule (Jackson Laboratory, Bar Harbor, ME) (40). Inducible kidney-specific *Cldn2* knockout mice were generated by crossing *Cldn2* floxed mice with mice carrying transgenes for Pax8-rtTA, which express the reverse tetracycline-dependent transactivator throughout the renal tubule (41), and for TRE-LC1, which express Cre recombinase under the control of an rtTA response element (42), kindly provided by Arohan Subramanya, University of Pittsburgh, with permission of the German Cancer Research Center (DKFZ). Recombination was induced by feeding doxycycline, 2 mg/ml with 2% sucrose in the drinking water for 7 days. Negative controls

were littermates with Pax8 or LC1 omitted, or that were fed 2% sucrose only. Mice were all fed standard lab chow *ad lib* (Teklad Rodent Diet 8604, Envigo).

Immunoblotting, immunofluorescence and histology

For protein immunoblots, whole kidney lysates were electrophoresed on sodium dodecyl sulfate-polyacrylamide gels, transferred to polyvinylidene difluoride membrane, and blotted with mouse anti-claudin-2 (ThermoFisher Scientific #32-5600, 1:500). Immunofluorescence was performed on frozen sections of paraformaldehyde perfusion-fixed kidneys as described previously (12). The primary antibodies used were mouse monoclonal claudin-2 (ThermoFisher 12H12) at 1:1000 for immunoblots, 1:500 for immunofluorescence, and ZO-1 (Santa Cruz SC-337250), 1:500. Histological staining was performed on paraffin-embedded sections with 2% Alizarin Red S (2% at pH 4.3 for 1-3 min) and Yasue metal substitution stain (43).

Blood and urine assays

Spot urine specimens were collected by spontaneous voiding onto a Parafilm mat. Mice were then anesthetized with isoflurane and blood was collected by cardiac puncture. Serum and urine calcium were measured by a colorimetric assay (Quantichrom, BioAssay Systems). Urine creatinine concentration was measured by the Jaffe reaction (Cayman Chemical). Plasma intact PTH (MicroVue Mouse PTH 1-84, Quidel, San Diego CA) and 1,25 dihydroxyvitamin D (Immunodiagnostic Systems) were measured by ELISA.

Systolic blood pressure and GFR

These were determined at 12–16 weeks of age. Systolic blood pressure and heart rate were determined in awake mice by an automated tail cuff system (BP-2000 Blood Pressure Analysis System, Visitech Systems, Apex, NC) for six consecutive days after appropriate training (44, 45). Precautions were taken to reduce the stress of the animals during automated tail cuff blood pressure measurements (46, 47). These included appropriate training of the mice over multiple days, prewarming to an ambient temperature of 29°C, measurement in a quiet, semi-darkened and clean environment, and performance of the measurements by one person and during a defined time of day when blood pressure is stable (between 1:00 and 3:00 pm).

GFR was determined between 9 am and 12 noon using plasma elimination kinetics of fluorescein isothiocyanate (FITC)-sinistrin (Fresenius-Kabi, Linz, Austria) measured by a transdermal detection system (NIC-Kidney Device, Medibeacon) (48). Briefly, under short and mild isoflurane anesthesia, a bolus dose of FITC-sinistrin (4%, 2 µl/g body weight in 0.85% NaCl) was injected into the retro-orbital plexus, followed by quick recovery of the mice from anesthesia. The transdermal signal was monitored before FITC-sinistrin injection and over 1.5 hrs after injection. Subsequently and after device readout (by MBLAB software, MPD Lab Version 2.2), the data were analyzed and GFR calculated using manufacturer software (MB Studio2).

Fractional lithium excretion

Twenty week old male mice were administered the loop diuretic bumetanide to inhibit lithium reabsorption in the thick ascending limb (40 mg/kg body weight i.p.; #B3023, Sigma-Aldrich; dissolved in ethanol and diluted in saline 1:10; 10 µl/g body weight). Thirty minutes later, the bladder was emptied by stimulating spontaneous urination and lithium chloride (LiCl, 5 mmol/kg body weight; #62476, Sigma-Aldrich; 2 µl/g body weight) injected by retro-orbital plexus injection under brief isoflurane anesthesia. The mice were subsequently housed in metabolic cages for timed urine collection for 1 hr. Plasma was collected from the tail tip at 3 min and 1 hr after LiCl injection. Lithium concentration in urine and plasma samples was determined by inductively-coupled plasma-mass spectrometry (Thermo iCAP RQ ICP-MS) at the Environmental and Complex Analysis Laboratory at the University of California San Diego. Plasma creatinine concentration was determined by isotope dilution liquid chromatography-tandem mass spectrometry at the O'Brien Center for Acute Kidney Injury Research at the University of Alabama at Birmingham (Birmingham, AL) and urine creatinine by a kinetic modification of Jaffe's reaction (ThermoFisher Scientific, Waltham, MA). Fractional urinary lithium excretion was determined as:

FE_{Li} = (Urine/Plasma Li)/(Urine/Plasma creatinine),

where plasma Li was the arithmetic mean of plasma lithium concentration measured at 3 min and 1 hr after LiCl injection.

Micro-CT analysis of kidneys

Kidneys were removed from mice, fixed and ethanol-dehydrated and then scanned with a high-resolution micro-computed tomography scanner. In the initial phase of the study, scans were acquired with a μ CT40 (Scanco Medical, Southeastern, PA) at 55 KeV and 6 μ m cubic resolutions, and renal calcifications assessed with a threshold of 220, as previously described (49). In the latter phase of the study, the scanner was switched to a Quantum GX2 microCT and imaged at 45 kV/88uA with a 0.5 mm Al filter. Three reference kidney samples were scanned on both scanners and used to normalize intensity values across experiments.

Micro-Fourier transform infrared spectroscopy (FTIR)

Kidney sections (5 μ m) were mounted on low-E glass slides (Kevley Technologies) for attenuated total internal reflection (ATR) imaging analysis. A serial section stained with Yasue silver replacement was used as a control section. Before infrared analysis, the control was visually examined with an Olympus white light microscope (x20 objective) to determine the areas of interest. Sections for ATR-FTIR imaging were not stained. ATR infrared images were collected with a PerkinElmer Spectrum Spotlight 400 infrared imaging microscope interfaced to a PerkinElmer FTIR spectrometer, as described previously (8). Each image (400 x 400 μ m area) had a spatial resolution of 1.56 μ m/pixel and contained 65,746 infrared spectra collected at a spectral resolution of 8 wavenumbers. Each spectrum in the image is the average of 4 individual scans. The images were further processed using Spectrum Image software (PerkinElmer).

Bone density measurements

Dual-energy X-ray absorptiometry (DEXA, Lunar PIXImus, GE Medical Systems) was used to measure bone mineral density in anesthetized mice at the indicated ages. The region of interest was adjusted to capture the density of the femur, lumbar vertebrae, or the whole body.

Quantitative RT-PCR

Whole tissue RNA was extracted with TRI Reagent (Sigma-Aldrich). First-strand cDNA iScript Reverse Transcription Supermix for RT-qPCR (Bio-Rad) was used for first-strand cDNA synthesis. mRNA quantitation was performed by Taqman assay using the ABI Prism 7900 HT Sequence Detection System (Applied Biosystems, Foster City, CA). Expression levels were normalized to ezrin. Threshold cycle (C_T) values were corrected for batch variation in amplification efficiency by using inter-run calibrator samples.

Diuretic challenge experiment

The protocol was modified from that described by Pei *et al* (50). Twelve week-old mice were acclimatized for 5 days in metabolic cages, then administered single intraperitoneal injections of furosemide (25 mg/kg body weight), hydrochlorothiazide (25 mg/kg body weight) or vehicle (2.5% NaOH in 0.9% NaCl) in a total volume of 10 µl per g body weight. Four hour collections of urine were taken at baseline, and immediately after each injection of diuretic or vehicle. During the protocol, mice were fed a gel-based diet (DietGel Recovery, ClearH₂O, Westbrook ME) to ensure adequate fluid intake.

Bulk chemical analysis of dissected kidney regions

Our method was adapted from protocols developed by Schmidt-Nielsen (51, 52) and Fenton (51) to determine sodium and urea concentrations in rodent kidney tissues. 16-17 week-old mice were first anesthetized and the kidney excised, decapsulated and cut into a block to expose a mid-coronal face. This was then sectioned perpendicular to the corticomedullary axis into pieces of tissue representing the papilla, the cortex and the segment of tissue in between, which included the entire outer medulla, and the base of the inner medulla. These were blotted on Whatman filter paper, transferred to microcentrifuge tubes and weighed. The time from excision of the whole kidney to isolation of all segments was ~2 minutes. Assuming, very conservatively, that tissue Ca^{2+} diffuses at the same rate as in free solution (diffusion coefficient at $4^{\circ}C \sim 5 \times 10^{-6}$ cm²/s, (53, 54)), the time required for 50% of Ca^{2+} to diffuse 1 mm is >30 min (55). So there should be reasonable preservation of any Ca^{2+} gradient within the time frame of the dissection. The tissue samples were then air-dried at $60^{\circ}C$ overnight over dessicant and reweighed.

To determine total calcium content by the "acid ash" method, dessicated tissue fragments were completely dissolved by adding 25 μ l of 35% nitric acid and 35% perchloric acid at 85°C, which generally took about 1 hour (56), then diluted in 75 μ l of water for assay. To determine diffusible calcium content, dessicated tissue fragments were suspended in 25 μ l of deionized water, heated to 90°C for 3 min, and incubated at 4°C for 18 hours to allow diffusion of calcium out of the tissue, and the aqueous solution taken for assay. Calcium

concentration was then assayed by a phenolsulphonephthalein-based colorimetric method (Quantichrom, BioAssay Systems).

Laser ablation inductively coupled time-of-flight mass spectrometry (LA-ICP-TOFMS)

Kidneys harvested from 6 week-old mice were snap-frozen in OCT using liquid nitrogen, sectioned into 10 μ m slices, and stored in -80° C. Elemental images were collected by LA-ICP-TOFMS using an imageBIO266 laser ablation laser ablation system interfaced with an Vitesse time-of-flight ICP-MS at the Biomedical National Elemental Imaging Resource (BNEIR). Spatial distributions of calcium, sodium and phosphorus were determined from the 44 Ca , 23 Na and 31 P isotope maps, respectively. Concentration profiles along the corticomedullary axis were determined from line scans at 100 μ m intervals. Complete details are provided in the Supplemental Methods and Suppl. Fig. 8.

Statistical analysis

Statistical analyses were performed with R version 4.2.1. Data for continuous variables are presented as mean ± standard error. Multi-way ANOVA was used to test for differences in multi-group experiments. Linear mixed effect models (LMM) with random intercept were used for experiments with repeated measurements because this method is robust to different numbers of measurements in different subjects and to missing values, and can generate interpretable coefficients. *P* values <0.05 were considered significant.

Study approval

All animal experiments were conducted in accordance with the National Institutes of Health Guide for the Care and Use of Laboratory Animals following protocol review and approval by the University of Kansas Medical Center and the Veterans Administration San Diego Healthcare System Institutional Animal Care and Use Committee.

Data availability

Values for all data points in graphs are reported in the Supporting Data Values file.

AUTHOR CONTRIBUTIONS

ASLY, CB AND DN designed the research study. CB, DN, OAG, SK, YCK, NL, HG, PSR, AJS, MNB and TP conducted the experiments. ASLY, DN, VV, APE, TP, BPJ and JCW analyzed the data. ASLY and CB drafted the manuscript, and all the authors reviewed and edited the manuscript.

FUNDING SUPPORT

This work is the result of NIH funding, in whole or in part, and is subject to the NIH Public Access Policy. Through acceptance of this federal funding, the NIH has been given a right to make the work publicly available in PubMed Central. This work was supported by NIH grant R01 DK115727 to ASLY, and by University of Alabama at Birmingham/University of California-San Diego O'Brien Center of Acute Kidney Injury NIH Grant P54 DK137307 and the Department of Veterans Affairs to VV. Laser ablation elemental imaging was performed at the Dartmouth Biomedical National Elemental Imaging Resource supported by NIGMS R24GM141194 and 1S10OD032352-01.

ACKNOWLEDGEMENTS

We thank Stephen Parnell and Heather Jackson for assistance with breeding and characterization of the mouse lines, the German Cancer Research Center (DKFZ) for permission to use the Pax8-rtTA mouse line, and Arohan Subramanya for sharing Pax8-LC1 mice and Jennifer Stashevsky for excellent histologic work.

REFERENCES

- 1. Tasian GE, Ross ME, Song L, Sas DJ, Keren R, Denburg MR, et al. Annual Incidence of Nephrolithiasis among Children and Adults in South Carolina from 1997 to 2012. *Clin J Am Soc Nephrol.* 2016;11(3):488-96.
- 2. Bushinsky DA, Coe FL, and Moe OW. In: Taal MW, Chertow GM, Marsden PA, Skorecki K, Yu AS, and Brenner BM eds. *Brenner and Rector's The Kidney*. Philadelphia: Elsevier; 2012:1455-507.
- 3. Pak CY, Oata M, Lawrence EC, and Snyder W. The hypercalciurias. Causes, parathyroid functions, and diagnostic criteria. *J Clin Invest.* 1974;54(2):387-400.
- Sutton RA, and Walker VR. Responses to hydrochlorothiazide and acetazolamide in patients with calcium stones. Evidence suggesting a defect in renal tubular function. The New England journal of medicine. 1980;302(13):709-13.
- 5. Coe FL, Favus MJ, Crockett T, Strauss AL, Parks JH, Porat A, et al. Effects of low-calcium diet on urine calcium excretion, parathyroid function and serum 1,25(OH)2D3 levels in patients with idiopathic hypercalciuria and in normal subjects. *The American journal of medicine*. 1982;72(1):25-32.
- 6. Weisinger JR. New insights into the pathogenesis of idiopathic hypercalciuria: the role of bone. *Kidney Int.* 1996;49(5):1507-18.
- 7. Randall R. Papillary pathology as precursor of primary renal calculus. *J Urol.* 1940;44:580-9.
- 8. Evan AP, Lingeman JE, Coe FL, Parks JH, Bledsoe SB, Shao Y, et al. Randall's plaque of patients with nephrolithiasis begins in basement membranes of thin loops of Henle. *The Journal of clinical investigation*. 2003;111(5):607-16.
- 9. Coe FL, Evan AP, Lingeman JE, and Worcester EM. Plaque and deposits in nine human stone diseases. *Urol Res.* 2010;38(4):239-47.
- 10. Suki WN. Calcium transport in the nephron. The American journal of physiology. 1979;237(1):F1-6.
- 11. Friedman PA. Mechanisms of renal calcium transport. Exp Nephrol. 2000;8(6):343-50.
- 12. Curry JN, Saurette M, Askari M, Pei L, Filla MB, Beggs MR, et al. Claudin-2 deficiency associates with hypercalciuria in mice and human kidney stone disease. *J Clin Invest.* 2020;130(4):1948-60.
- 13. Beggs MR, Young K, Pan W, O'Neill DD, Saurette M, Plain A, et al. Claudin-2 and claudin-12 form independent, complementary pores required to maintain calcium homeostasis. *Proc Natl Acad Sci U S A*. 2021;118(48).
- 14. van Abel M, Hoenderop JG, van der Kemp AW, Friedlaender MM, van Leeuwen JP, and Bindels RJ. Coordinated control of renal Ca(2+) transport proteins by parathyroid hormone. *Kidney Int.* 2005;68(4):1708-21.
- 15. Tournus M, Seguin N, Perthame B, Thomas SR, and Edwards A. A model of calcium transport along the rat nephron. *American journal of physiology Renal physiology*. 2013;305(7):F979-94.
- 16. Worcester EM, Coe FL, Evan AP, Bergsland KJ, Parks JH, Willis LR, et al. Evidence for increased postprandial distal nephron calcium delivery in hypercalciuric stone-forming patients. *American journal of physiology Renal physiology*. 2008;295(5):F1286-94.
- 17. Worcester EM, and Coe FL. Evidence for altered renal tubule function in idiopathic calcium stone formers. *Urol Res.* 2010;38(4):263-9.
- 18. Ko B, Bergsland K, Gillen DL, Evan AP, Clark DL, Baylock J, et al. Sex differences in proximal and distal nephron function contribute to the mechanism of idiopathic hypercalcuria in calcium stone formers. *Am J Physiol Regul Integr Comp Physiol.* 2015;309(1):R85-92.
- 19. Coe FL, Evan A, and Worcester E. Pathophysiology-based treatment of idiopathic calcium kidney stones. *Clinical journal of the American Society of Nephrology : CJASN.* 2011;6(8):2083-92.
- 20. Hoenderop JG, van Leeuwen JP, van der Eerden BC, Kersten FF, van der Kemp AW, Merillat AM, et al. Renal Ca2+ wasting, hyperabsorption, and reduced bone thickness in mice lacking TRPV5. *J Clin Invest*. 2003;112(12):1906-14.
- 21. Hou J, Shan Q, Wang T, Gomes AS, Yan Q, Paul DL, et al. Transgenic RNAi depletion of claudin-16 and the renal handling of magnesium. *J Biol Chem.* 2007;282(23):17114-22.
- 22. Hou J, Renigunta A, Gomes AS, Hou M, Paul DL, Waldegger S, et al. Claudin-16 and claudin-19 interaction is required for their assembly into tight junctions and for renal reabsorption of magnesium. *Proc Natl Acad Sci U S A.* 2009;106(36):15350-5.

- 23. Will C, Breiderhoff T, Thumfart J, Stuiver M, Kopplin K, Sommer K, et al. Targeted deletion of murine Cldn16 identifies extra- and intrarenal compensatory mechanisms of Ca2+ and Mg2+ wasting. *Am J Physiol Renal Physiol.* 2010;298(5):F1152-61.
- 24. Loh NY, Bentley L, Dimke H, Verkaart S, Tammaro P, Gorvin CM, et al. Autosomal dominant hypercalciuria in a mouse model due to a mutation of the epithelial calcium channel, TRPV5. *PLoS One.* 2013;8(1):e55412.
- 25. Evan AP, Bledsoe SB, Smith SB, and Bushinsky DA. Calcium oxalate crystal localization and osteopontin immunostaining in genetic hypercalciuric stone-forming rats. *Kidney Int.* 2004;65(1):154-61.
- 26. Breiderhoff T, Himmerkus N, Stuiver M, Mutig K, Will C, Meij IC, et al. Deletion of claudin-10 (Cldn10) in the thick ascending limb impairs paracellular sodium permeability and leads to hypermagnesemia and nephrocalcinosis. *Proc Natl Acad Sci U S A.* 2012;109(35):14241-6.
- 27. Martin M, Hadj Aissa A, Baverel G, and Pellet M. [Intrarenal distribution of calcium and magnesium in the dog. Effect of an osmotic diuresis (author's transl)]. *J Physiol (Paris)*. 1975;70(2):159-72.
- 28. Hautmann R, Lehmann A, and Komor S. Intrarenal distribution of oxalic acid, calcium, sodium, and potassium in man. *Eur J Clin Invest.* 1980;10(2 Pt 1):173-6.
- 29. Hautmann R, Lehmann A, and Komor S. Calcium and oxalate concentrations in human renal tissue: the key to the pathogenesis of stone formation? *J Urol.* 1980;123(3):317-9.
- 30. Low RK, and Stoller ML. Endoscopic mapping of renal papillae for Randall's plaques in patients with urinary stone disease. *J Urol.* 1997;158(6):2062-4.
- 31. Randall A. The Origin and Growth of Renal Calculi. *Ann Surg.* 1937;105(6):1009-27.
- 32. Evan AP, Coe FL, Lingeman JE, Bledsoe SB, and Worcester EM. Randall's Plaque in Stone Formers Originates in Ascending Thin Limbs. *Am J Physiol Renal Physiol.* 2018.
- 33. Coe FL, Worcester EM, and Evan AP. Idiopathic hypercalciuria and formation of calcium renal stones. *Nat Rev Nephrol.* 2016;12(9):519-33.
- 34. Linnes MP, Krambeck AE, Cornell L, Williams JC, Jr., Korinek M, Bergstralh EJ, et al. Phenotypic characterization of kidney stone formers by endoscopic and histological quantification of intrarenal calcification. *Kidney Int.* 2013;84(4):818-25.
- 35. Verrier C, Bazin D, Huguet L, Stephan O, Gloter A, Verpont MC, et al. Topography, Composition and Structure of Incipient Randall Plaque at the Nanoscale Level. *J Urol.* 2016;196(5):1566-74.
- 36. Rocha AS, Magaldi JB, and Kokko JP. Calcium and phosphate transport in isolated segments of rabbit Henle's loop. *J Clin Invest.* 1977;59(5):975-83.
- 37. Enck AH, Berger UV, and Yu AS. Claudin-2 is selectively expressed in proximal nephron in mouse kidney. *Am J Physiol Renal Physiol*. 2001;281(5):F966-74.
- 38. Torres-Pinzon DL, Ralph DL, Veiras LC, and McDonough AA. Sex-specific adaptations to high-salt diet preserve electrolyte homeostasis with distinct sodium transporter profiles. *Am J Physiol Cell Physiol.* 2021;321(5):C897-C909.
- 39. Veiras LC, Girardi ACC, Curry J, Pei L, Ralph DL, Tran A, et al. Sexual Dimorphic Pattern of Renal Transporters and Electrolyte Homeostasis. *J Am Soc Nephrol*. 2017;28(12):3504-17.
- 40. Bouchard M, Souabni A, and Busslinger M. Tissue-specific expression of cre recombinase from the Pax8 locus. *Genesis*. 2004;38(3):105-9.
- 41. Traykova-Brauch M, Schonig K, Greiner O, Miloud T, Jauch A, Bode M, et al. An efficient and versatile system for acute and chronic modulation of renal tubular function in transgenic mice. *Nat Med.* 2008;14(9):979-84.
- 42. Schonig K, Schwenk F, Rajewsky K, and Bujard H. Stringent doxycycline dependent control of CRE recombinase in vivo. *Nucleic Acids Res.* 2002;30(23):e134.
- 43. Yasue T. Histochemical identification of calcium oxalate. Acta Histochem Cytochem. 1969;2(3):83-95.
- 44. Onishi A, Fu Y, Patel R, Darshi M, Crespo-Masip M, Huang W, et al. A role for tubular Na(+)/H(+) exchanger NHE3 in the natriuretic effect of the SGLT2 inhibitor empagliflozin. *Am J Physiol Renal Physiol.* 2020;319(4):F712-F28.
- 45. Song P, Huang W, Onishi A, Patel R, Kim YC, van Ginkel C, et al. Knockout of Na(+)-glucose cotransporter SGLT1 mitigates diabetes-induced upregulation of nitric oxide synthase NOS1 in the macula densa and glomerular hyperfiltration. *Am J Physiol Renal Physiol.* 2019;317(1):F207-F17.
- 46. Meneton P, Ichikawa I, Inagami T, and Schnermann J. Renal physiology of the mouse. *Am J Physiol Renal Physiol.* 2000;278(3):F339-F51.
- 47. Krege JH, Hodgin JB, Hagaman JR, and Smithies O. A noninvasive computerized tail-cuff system for measuring blood pressure in mice. *Hypertension*. 1995;25(5):1111-5.

- 48. Crespo-Masip M, Goodluck HA, Kim YC, Oe Y, Roach AM, Kanoo S, et al. ASK1 limits kidney glucose reabsorption, growth, and mid-late proximal tubule KIM-1 induction when diabetes and Western diet are combined with SGLT2 inhibition. *Am J Physiol Renal Physiol.* 2025;328(5):F662-F75.
- 49. Zelenchuk LV, Hedge AM, and Rowe PS. SPR4-peptide alters bone metabolism of normal and HYP mice. *Bone*. 2015;72:23-33.
- 50. Pei L, Solis G, Nguyen MT, Kamat N, Magenheimer L, Zhuo M, et al. Paracellular epithelial sodium transport maximizes energy efficiency in the kidney. *J Clin Invest.* 2016;126(7):2509-18.
- 51. Fenton RA, Chou CL, Stewart GS, Smith CP, and Knepper MA. Urinary concentrating defect in mice with selective deletion of phloretin-sensitive urea transporters in the renal collecting duct. *Proc Natl Acad Sci U S A.* 2004;101(19):7469-74.
- 52. Schmidt-Nielsen B, Graves B, and Roth J. Water removal and solute additions determining increases in renal medullary osmolality. *Am J Physiol*. 1983;244(5):F472-82.
- 53. Robinson RA, and Chia CL. The diffusion coefficient of calcium chloride in aqueous solution. *J Am Chem Soc.* 1952;74(11):2776-7.
- 54. Robinson RA, and Stokes RH. *Electrolyte Solutions*. Mineola, NY: Dover; 1959.
- 55. Macey RI. In: Andreoli TE, Hoffman JF, Fanestil DD, and Schultz SG eds. *Membrane Physiology*. New York: Plenum; 1987:111-31.
- 56. Kim M, Sessler NE, Tembe V, Favus MJ, and Bushinsky DA. Response of genetic hypercalciuric rats to a low calcium diet. *Kidney Int.* 1993;43:189-96.

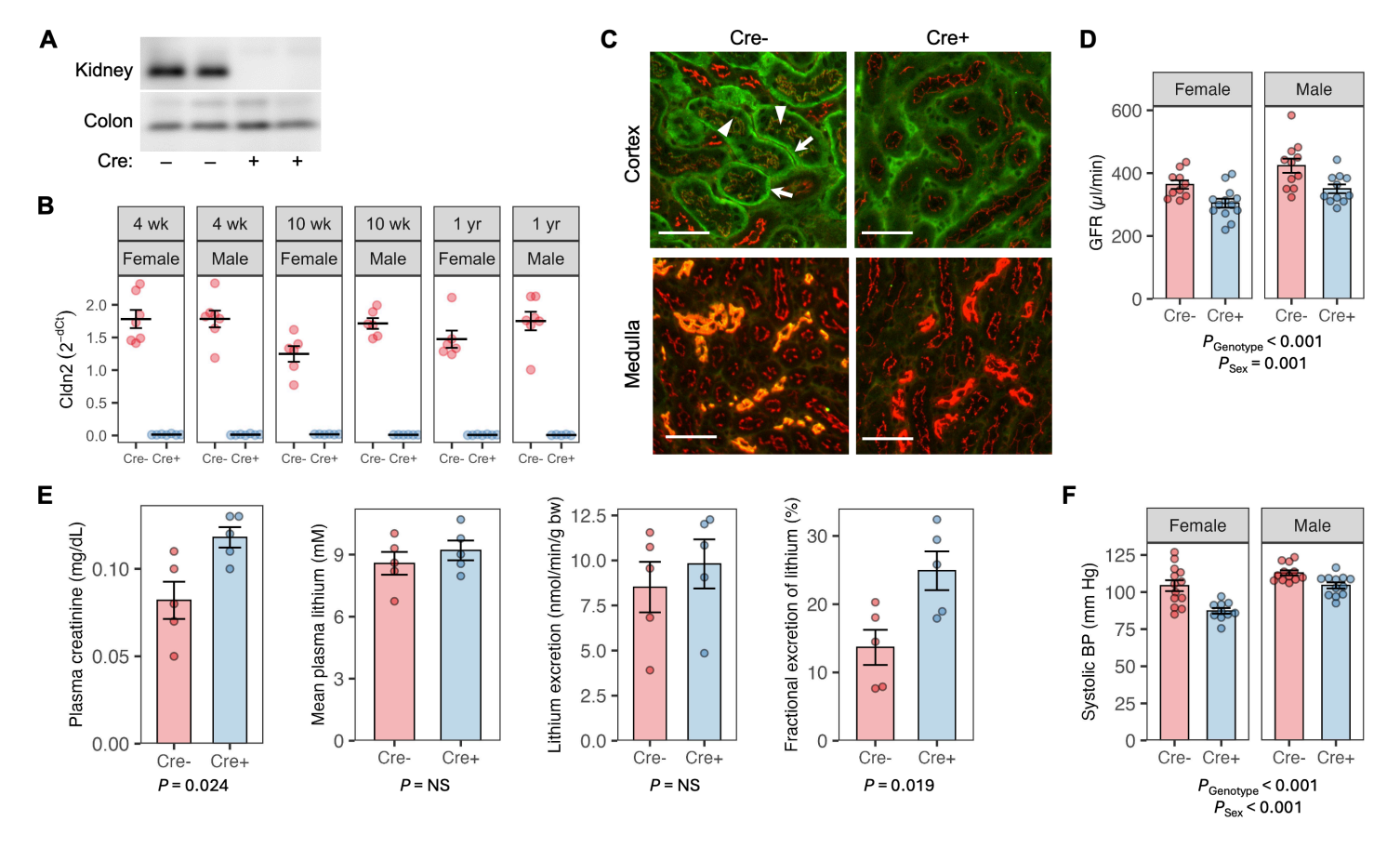


Fig. 1. General phenotype of constitutive, kidney-specific Cldn2 knockout mice. **A.** Western blot for claudin-2 in kidney and colon tissue from knockout mice (Cre+) and control littermates (Cre-). **B.** Cldn2 mRNA expression by quantitative PCR in kidneys, relative to ezrin, plotted as $2^{-\Delta Ct}$ values. Differences are significant for genotype (P < 0.001), age (P = 0.03 for 10 wk vs. 4 wk) and sex (P = 0.04) by 3-way ANOVA. **C.** Immunofluorescence staining of kidney cortex and medulla with antibodies to claudin-2 (green) and ZO-1 (red). Orange/yellow fluorescence indicates colocalization of claudin-2 with ZO-1. Claudin-2 is detectable at the tight junctions (arrowheads) and basolateral membrane (arrow) of proximal tubules in the cortex, and in thin descending limbs in the medulla of Cre- control mice but not Cre+ knockout mice. Scale bar: 50 μm. **D.** GFR determined from FITC-sinistrin clearance. N = 10-13 per group. **E.** Determination of fractional excretion of lithium. Following pretreatment with bumetanide to block thick ascending limb sodium and lithium transport, male mice were given an i.v. bolus of LiCl and plasma creatinine concentration, plasma lithium (mean of samples 3 min and 60 min post-injection) and lithium excretion in a 1 hr urine collection were determined. N = 5 per group. **F.** Systolic blood pressure determined by tail cuff measurement. N = 10-13 per group.

FIGURE 2

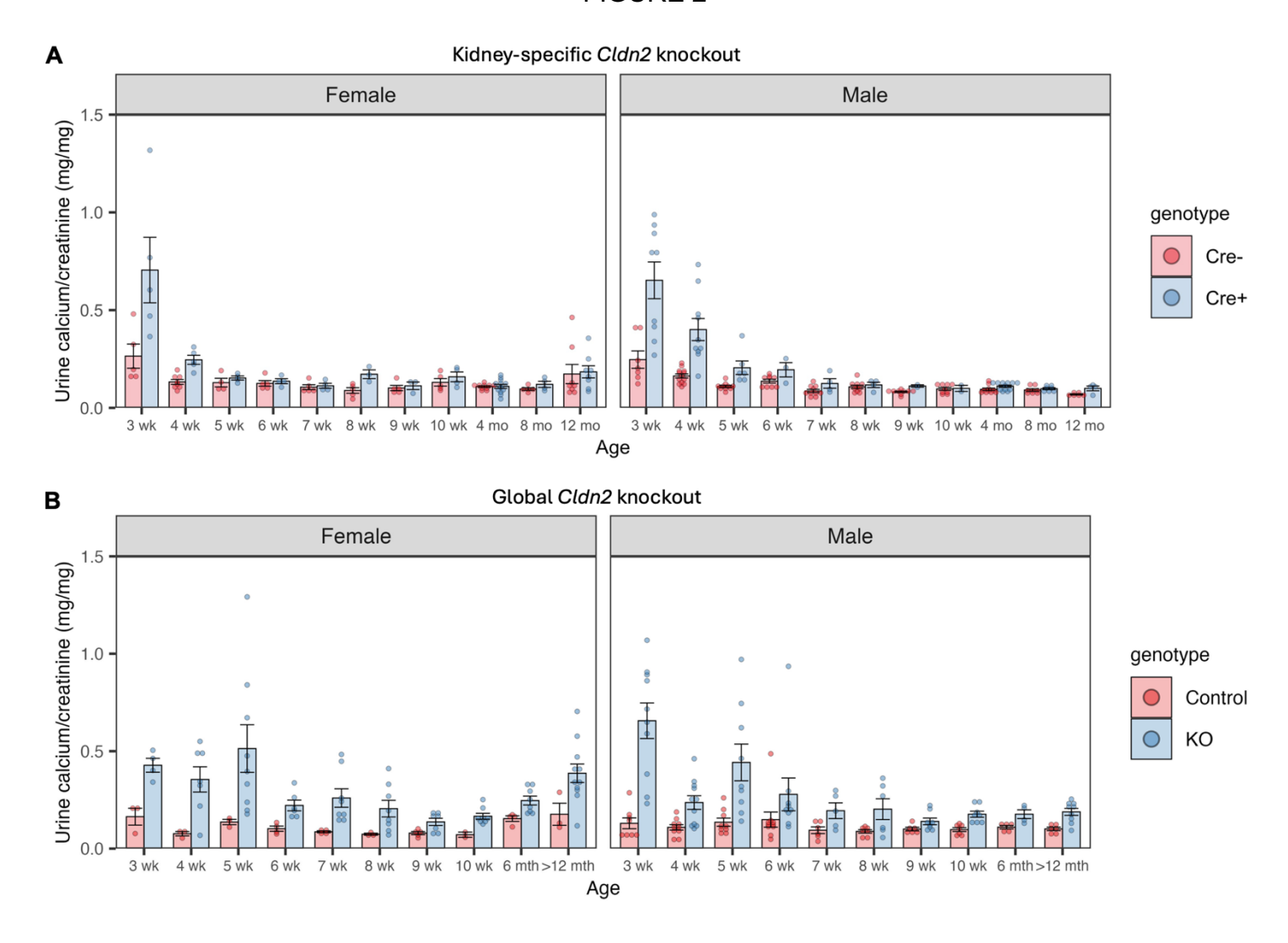


Fig. 2. Elevated urine calcium excretion in young but not older *Cldn2* knockout mice. **A.** Urine calcium/creatinine ratio in kidney-specific *Cldn2* knockout mice. Levels are higher in Cre+ mice compared to Cre- (least squares mean difference \pm SE = 0.143 \pm 0.046, P = 0.002) and decrease more rapidly with age (P = 0.002 for genotype*age interaction) with no difference between the sexes, using LMM. **B.** Urine calcium/creatinine ratio in global, constitutive *Cldn2* knockout mice. Levels are higher in knockout mice than control littermates (least squares mean difference \pm SE = 0.193 \pm 0.039, P < 0.001), but there is no significant interaction with age. Age group >12 mth included mice ranging from 63 to 101 weeks old. N = 2–13 per group.

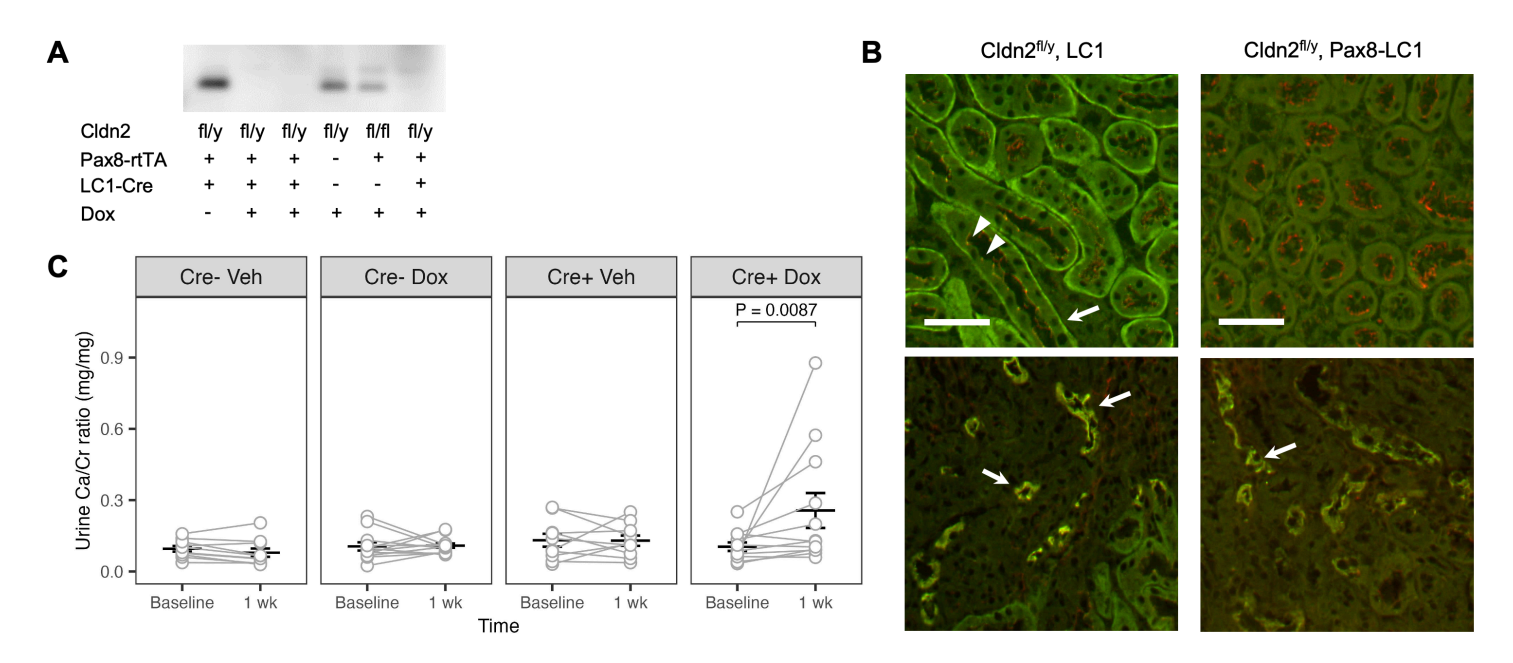


Fig. 3. Induction of hypercalciuria within a week in inducible kidney-specific *Cldn2* knockout mice. **A.** Western blot for claudin-2 in whole kidney lysates from knockout mice (*Cldn2*^{fl/y}, Pax8-LC1) treated with doxycycline (Dox) or vehicle (lane 1) and control littermates without the Pax8 and/or LC1 genes (lanes 4 & 5). **B.** Immunofluorescence staining of kidney sections with antibodies to claudin-2 (green) and ZO-1 (red). The upper panels show kidney cortex, where claudin-2 is detectable at the tight junctions (arrowheads) and basolateral membrane (arrow) of proximal tubules in the control mouse (*left*) and absent in the knockout mouse (*right*). The lower panels show the inner stripe of outer medulla, where claudin-2 localized to the thin descending limbs (arrows) is only mildly reduced in the knockout compared to control. Claudin-2 deletion in the thin descending limbs was incomplete even after 3 weeks of doxycycline induction (not shown). Scale bar: 50 μm. **C.** Urine calcium/creatinine (Ca/Cr) ratio before and after 1 week of doxycycline (Dox) or vehicle (Veh) in inducible knockout mice (Cre+) or control littermates without LC1 (Cre-). Bars represent mean ± SEM. *P* value is shown for interaction of time with the group, Cre+ Dox, by repeated measures LMM.

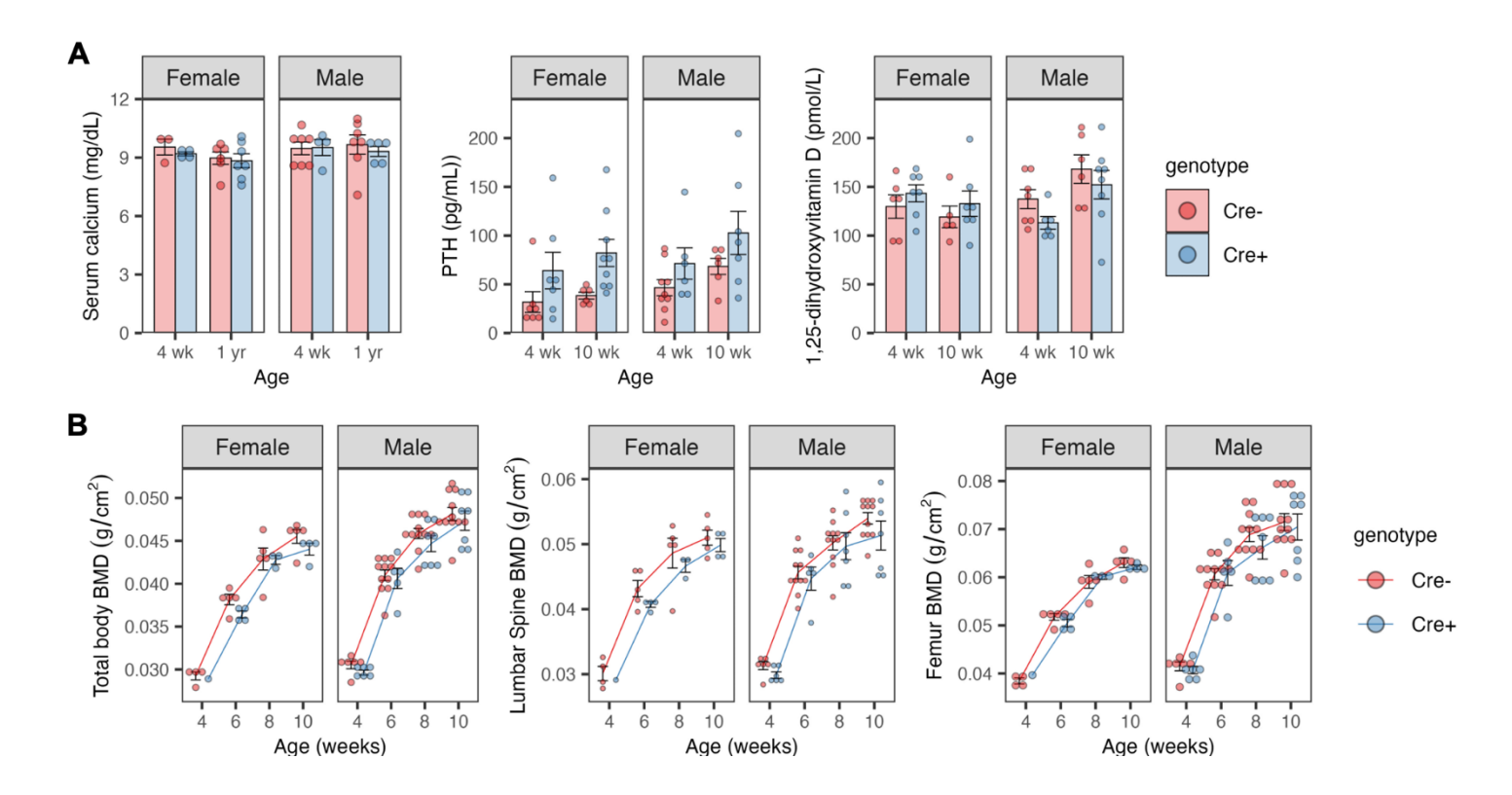


Fig. 4. Analysis of response to hypercalciuria in constitutive kidney-specific Cldn2 knockout mice shows compensatory upregulation of PTH. **A.** Serum calcium, intact PTH and 1,25-dihydroxyvitamin D levels. N = 3–9 per group. **B.** Total body, lumbar spine and femur bone mineral density (BMD) between 4 and 10 weeks of age. N = 4–11 in all groups except 4 week-old Cre+ female (N = 1). P = 0.0008 for the effect of genotype on PTH levels by 3-way ANOVA. For all other measures, P is non-significant for genotype and its interactions with sex and age.

FIGURE 5

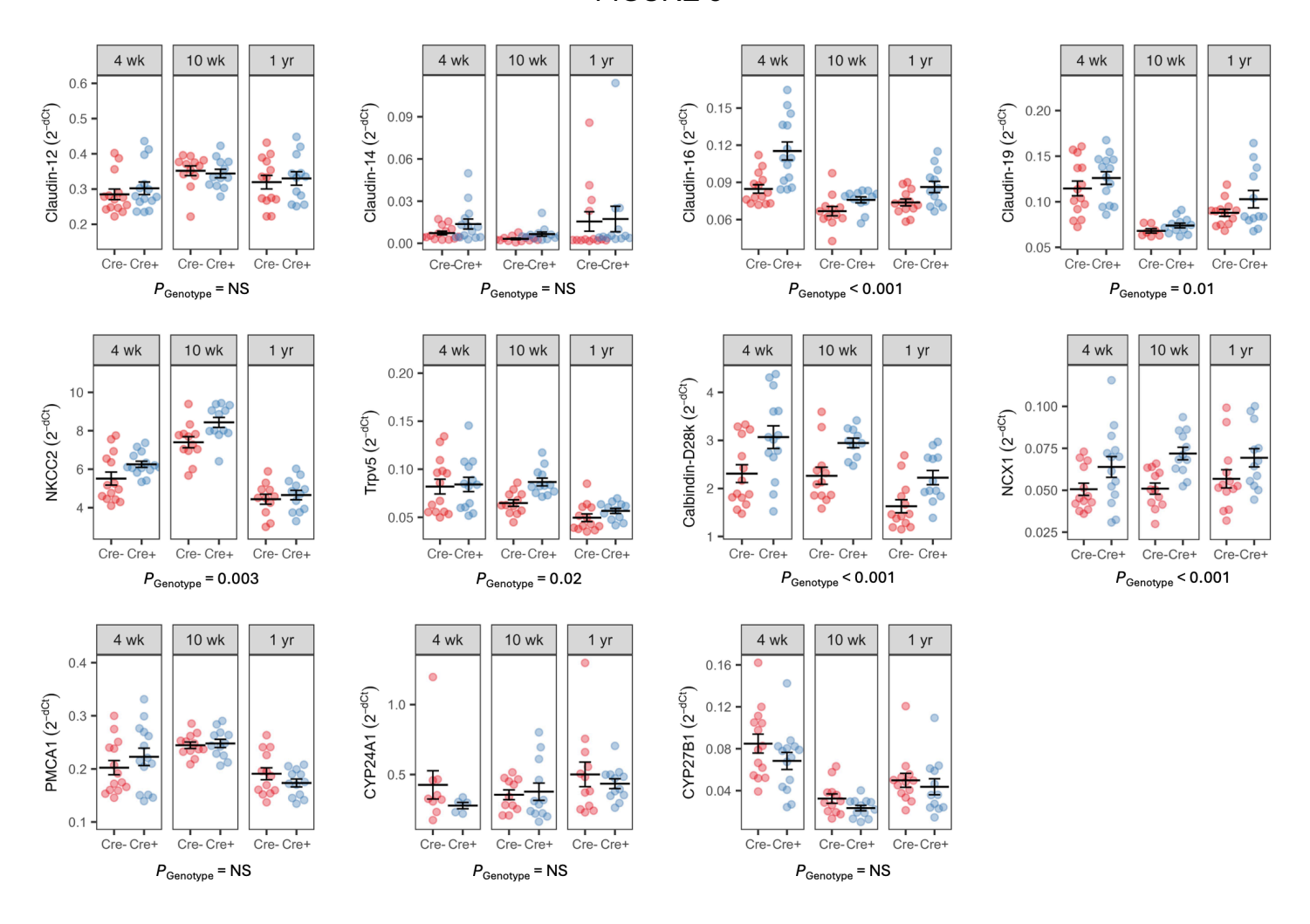


Fig. 5. Compensatory upregulation of mRNA expression of thick ascending limb and distal convoluted tubule calcium transporters in constitutive kidney-specific *Cldn2* knockout mice. Expression levels for each gene by quantitative PCR, relative to ezrin, are plotted as $2^{-\Delta Ct}$ values. *P* values are reported for differences between genotype (Cre+ vs. Cre-) by 3-way ANOVA with between-group factors of age, sex and genotype. Sex as a factor was not significant so males and females are grouped for display. N = 6–7 per age group and genotype.

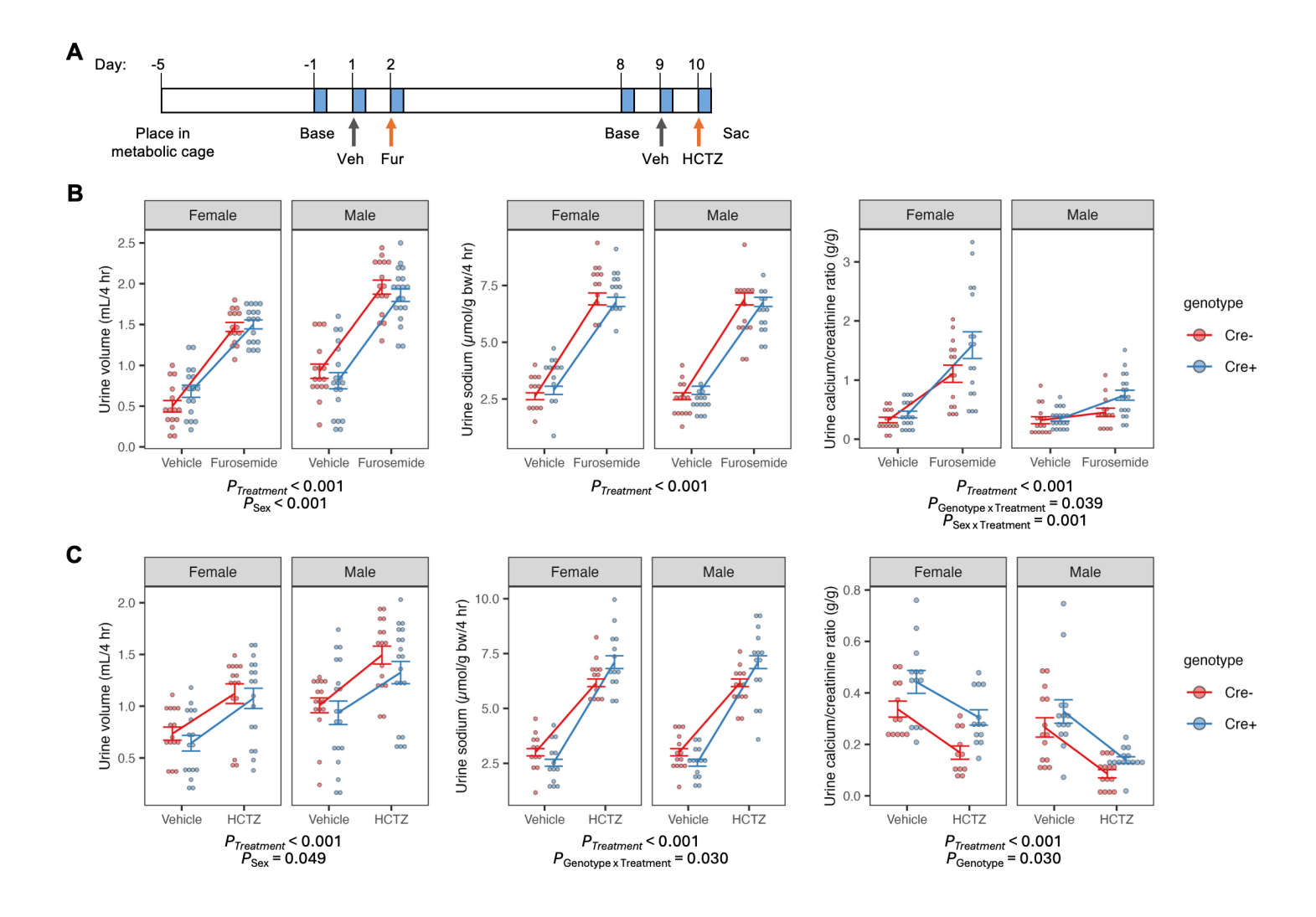


Fig. 6. Diuretic challenge assay unmasks enhanced thick ascending limb calcium reabsorption in constitutive kidney-specific *Cldn2* knockout mice. **A.** Diagram of experimental protocol. Four-hour urine collections (blue) were taken at baseline (Base) a day prior to sequential injections with vehicle (Veh) followed the next day with diuretic, either furosemide (Fur) or hydrochlorothiazide (HCTZ). The two diuretics were separated by an interval of one week. Diet was switched to gel formulation at Day -1 to ensure adequate hydration. Effect of furosemide (**B**) and hydrochlorothiazide (**C**) compared to vehicle on urine volume, sodium excretion and calcium excretion are shown. Urine measurements were modeled by LMM with between-subject effects of genotype and sex, within-subject effect of treatment, and the interaction of genotype and sex with treatment. N = 15–19 per group. The statistically significant fixed effects are listed below each panel.

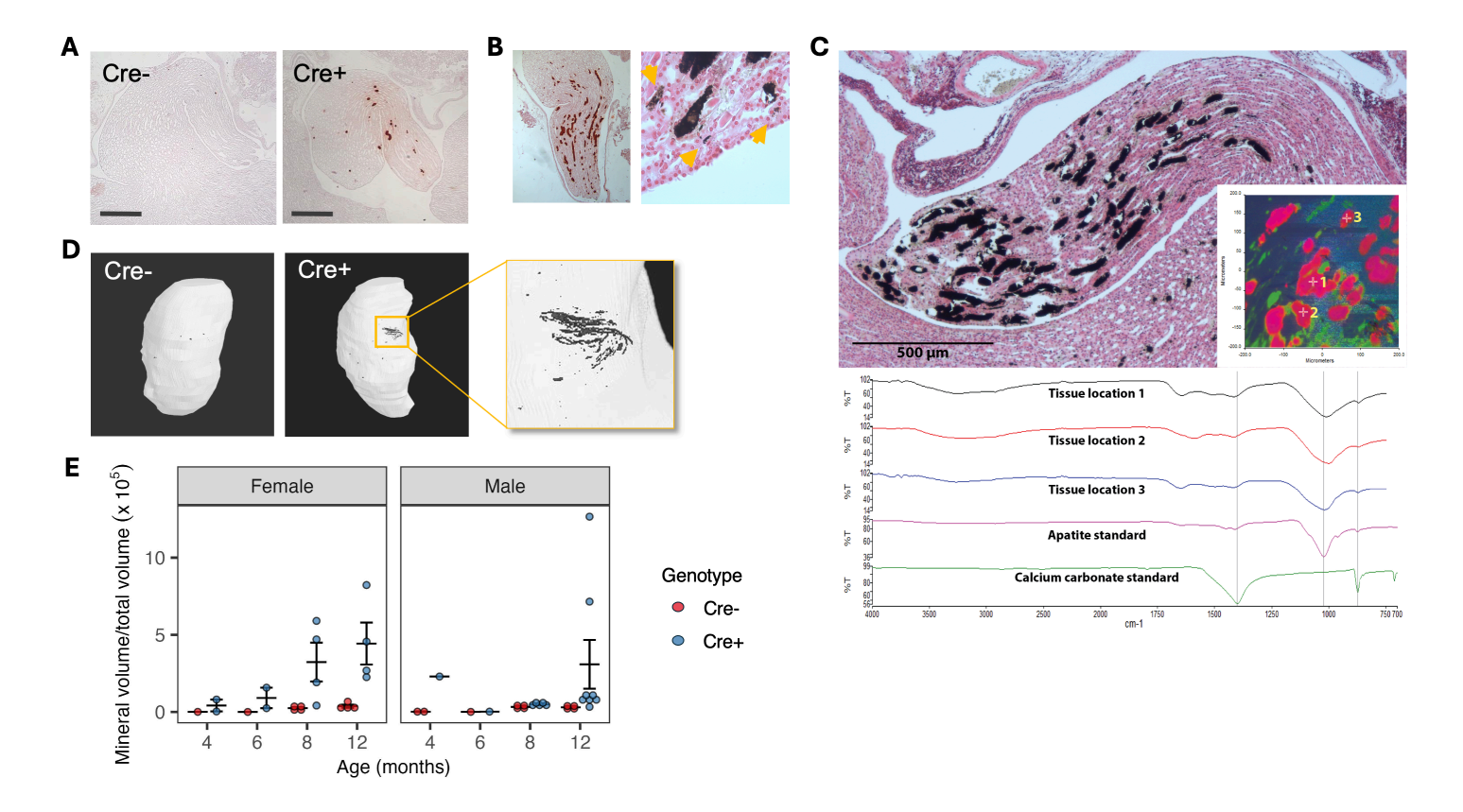


Fig. 7. Nephrocalcinosis in older kidney-specific *Cldn2* knockout mice. **A.** Alizarin Red staining of the renal inner medulla of 1 year-old female Cre– and Cre+ mice. **B.** *Left:* Papilla of a 16 month-old female Cre+ mouse stained with Alizarin Red. *Right:* High magnification view of Yasue-stained section showing large intratubular plugs and smaller interstitial granular deposits (yellow arrows). **C.** Infrared analysis of mineral deposits. *Upper panel:* Yasue-stained section showing extensive mineral deposition in renal papilla. *Inset:* False color representation of spectrum field with infrared microscope; square is 400 x 400 μm. *Lower panel:* Spectra from mineral locations 1-3, indicated in inset, along with standard spectra for apatite and calcite (calcium carbonate). **D.** Micro-CT scans of the kidneys from A. at bone density setting to detect mineral deposits. **E.** Quantitation of mineral volume as a proportion of total kidney volume (*P* = 0.0036 for effect of genotype by 3-way ANOVA).

FIGURE 8

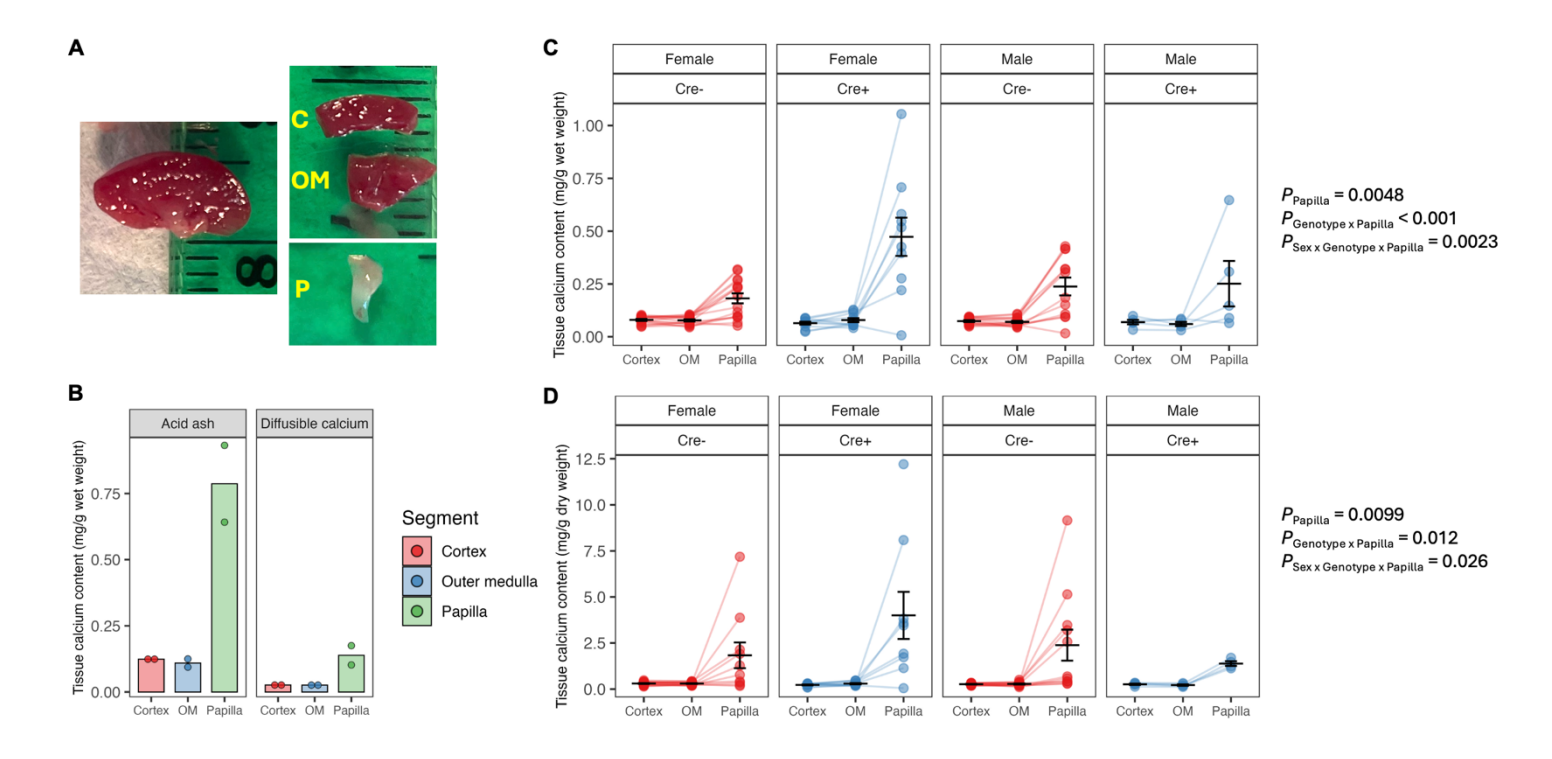


Fig. 8. Enhanced papillary Ca content in 4-6 months old kidney-specific claudin-2 knockout mice. Bulk chemical analysis of the axial distribution of tissue calcium in mouse kidney. **A.** Dissection of mouse kidney. Coronal section through kidney on left, and dissection of three regions on right. C, cortex; OM, outer medulla and base of inner medulla; P, papilla. Small tick marks on the ruler represent 1 mm intervals. **B.** Comparison of two methods of tissue calcium extraction (acid ash and diffusible calcium) in wild-type mice. **C., D.** Kidney calcium content relative to tissue wet weight (**C**) or dry weight (**D**) in kidney-specific claudin-2 knockout mice (Cre+) as compared to control littermates (Cre-). Data were analyzed with multi-level, mixed effect models with kidney region as the Level 1 unit, nested within individual mice as Level 2. Statistically significant P values are reported for the fixed effects of kidney region (papilla or outer medulla, relative to cortex as the reference), genotype and sex and their interactions. N = 3-9 mice per group.

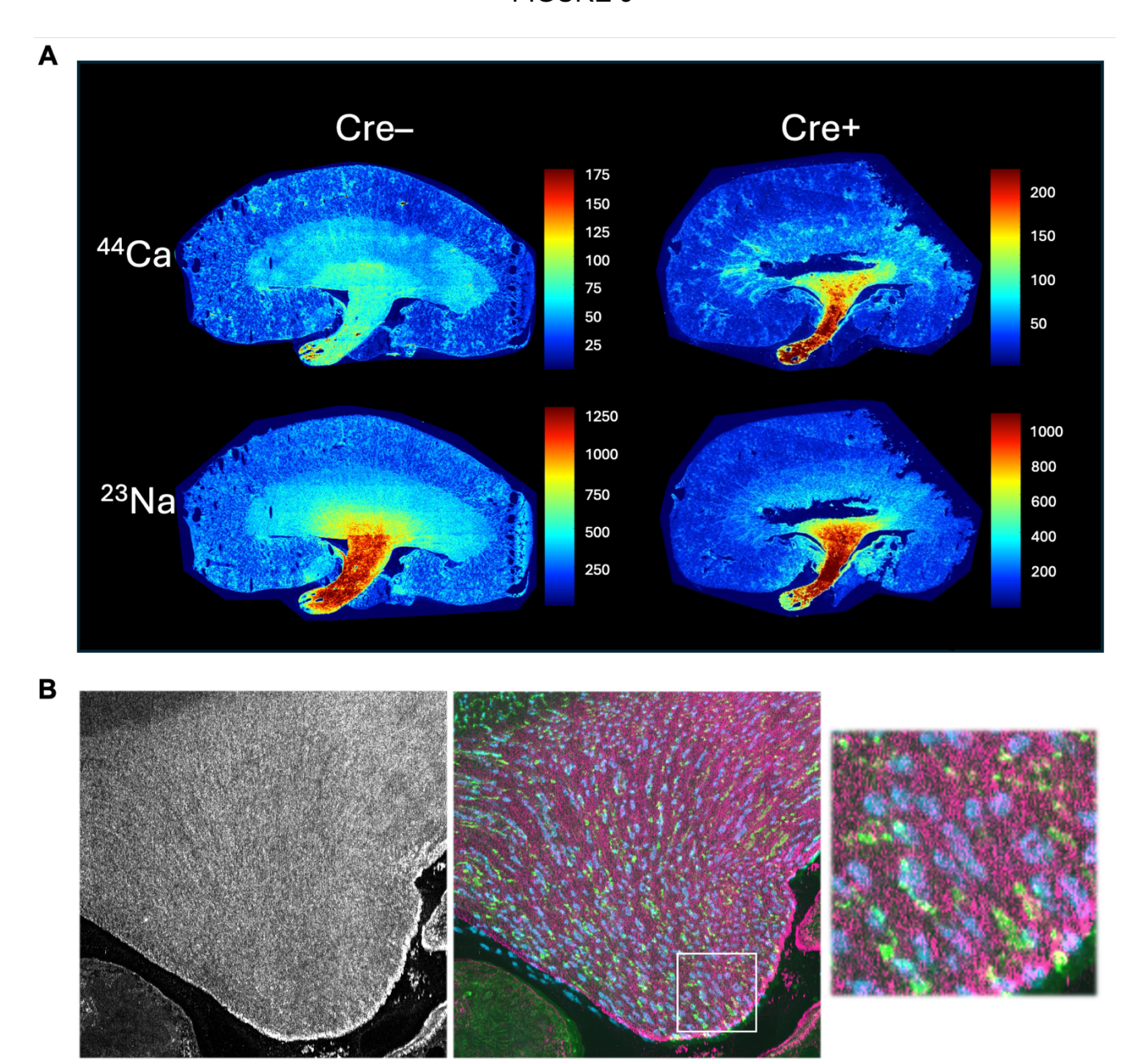


Fig. 9. Elemental mapping by LA-ICP MS in 6 week-old mouse kidneys. **A.** 2D maps of calcium (⁴⁴Ca) and sodium (²³Na) in midline coronal kidney sections of *Cldn2* kidney-specific knockout (Cre+) and control (Cre–) mouse. Color scale depicts concentration in ppm. **B.** High resolution image of a Cre+ mouse papilla. *Left panel:* ⁴⁴Ca map at 2 μm resolution. *Middle panel:* Overlay of ⁴⁴Ca map (magenta) with immunofluorescence labeling of an adjacent section with AQP1 (green) and AQP2 (cyan). Region delineated by white square is magnified in the *right panel.* The stippled pattern of calcium is consistent with the size of individual laser spots and consistent with a uniform distribution.

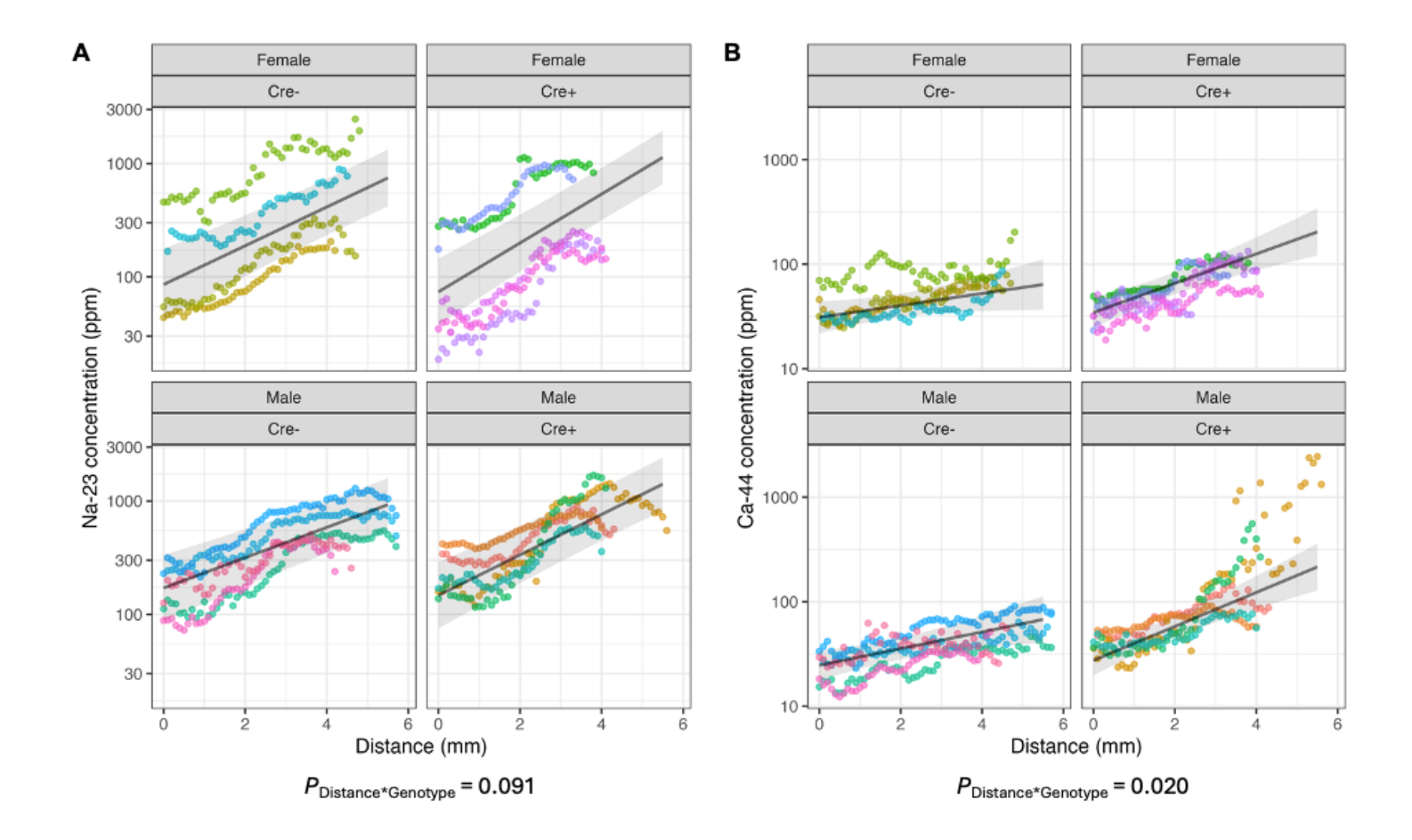


Fig. 10. Elemental corticomedullary concentration profiles for 23 Na (**A**) and 44 Ca (**B**). Element concentrations in parts per million (ppm) are plotted on a log scale. Distance is measured from the cortical surface in millimeters. Kidney sections from each individual mouse are represented by a different color (N = 4–5 mice per group). Black lines and shaded bands represent the linear mixed model predictions from marginal means and their 95% confidence intervals. P values are reported for slope of log-concentration vs. distance.